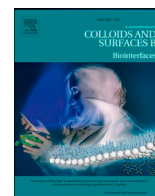




Since January 2020 Elsevier has created a COVID-19 resource centre with free information in English and Mandarin on the novel coronavirus COVID-19. The COVID-19 resource centre is hosted on Elsevier Connect, the company's public news and information website.

Elsevier hereby grants permission to make all its COVID-19-related research that is available on the COVID-19 resource centre - including this research content - immediately available in PubMed Central and other publicly funded repositories, such as the WHO COVID database with rights for unrestricted research re-use and analyses in any form or by any means with acknowledgement of the original source. These permissions are granted for free by Elsevier for as long as the COVID-19 resource centre remains active.



Injectable niclosamide nanohybrid as an anti-SARS-CoV-2 strategy

N. Sanoj Rejinold^a, Huiyan Piao^a, Geun-woo Jin^b, Go Eun Choi^{a,c,d,*}, Jin-Ho Choy^{a,e,f,*}

^a Intelligent NanoHybrid Materials Laboratory (INML), Institute of Tissue Regeneration Engineering (ITREN), Dankook University, Cheonan, 31116, Republic of Korea

^b R&D Center, CnPharm Co., LTD., Seoul, 03759, Republic of Korea

^c College of Science and Technology, Dankook University, Cheonan, 31116, Republic of Korea

^d Department of Nanobiomedical Science and BK21 PLUS NBM Global Research Center for Regenerative Medicine, Dankook University, Cheonan, 31116, Republic of Korea

^e Department of Pre-Medical Course, College of Medicine, Dankook University, Cheonan, 31116, Republic of Korea

^f Tokyo Tech World Research Hub Initiative (WRHI), Institute of Innovative Research, Tokyo Institute of Technology, Yokohama, 226-8503, Japan

ARTICLE INFO

Keywords:

COVID-19

Injectable formulation

BSA

PEG

In-vivo

ABSTRACT

COVID-19 is a rapidly evolving emergency, which necessitates scientific community to come up with novel formulations that could find quick relief to the millions affected around the globe. Remdesivir being the only injectable drug by FDA for COVID-19, it initially showed promising results, however, later on failed to retain its claims, hence rejected by the WHO. Therefore, it is important to develop injectable formulation that are effective and affordable. Here in this work, we formulated poly ethylene glycol (PEG) coated bovine serum albumin (BSA) stabilized Niclosamide (NIC) nanoparticles (NPs) (~BSA-NIC-PEG NPs) as an effective injectable formulation. Here, serum albumin mediated strategy was proposed as an effective strategy to specifically target SARS-CoV-2, the virus that causes COVID-19. The *in-vitro* results showed that the developed readily water dispersible formulation with a particle size <120 nm size were well stable even after 3 weeks. Even though the *in-vitro* studies showed promising results, the *in-vivo* pharmacokinetic (PK) study in rats demands the need of conducting further experiments to specifically target the SARS-CoV-2 in the virus infected model. We expect that this present formulation would be highly preferred for targeting hypoalbuminemia conditions, which was often reported in elderly COVID-19 patients. Such studies are on the way to summarize its potential applications in the near future.

1. Introduction

COVID-19 has been affecting 204 M individual all around the world leaving 4.32 M into fatal deaths as of Aug 12-2021. Additionally, the new genetic variant of COVID-19 making the current situation worse than ever before ever since it was first reported in the UK [1]. Therefore, it is urgent to discover new anti-viral medicines, which could be combined along with the ongoing global vaccinations. Remdesivir is the only injectable formulation for COVID-19 [2–8], with promising results in the beginning, however, the drug had controversial results since it showed no or negligible results in COVID-19 patient studies, thereby WHO later declared its ineffectiveness [9]. Therefore, developing novel formulations are very urgent. On the other hand, FDA approved anthelmintic NIC [10] has shown anti-viral properties among other FDA approved drug molecules in the *in-vitro* experiments on SARS-CoV-2 infected VERO cells. It was reported that even a small dosage of 0.16 μM of NIC

(57.14 ng/mL) could induce potential anti-viral effects on SARS-CoV-2 infected VERO cells [11]. However, the major limitation of NIC is associated with its poor water solubility, thereby low bioavailability [12].

NIC has been extensively studied for anti-cancer [13,14], anti-inflammatory [15] and anti-viral potency [16]. It has shown significant anti-viral effects on wide variety of viral pathologies including MERS [17], SARS [18], the similar family of COVID-19. The major mechanisms involved in NIC antiviral potency against SARS-CoV-2 are as follows: 1) inhibiting endocytosis; 2) inhibiting autophagy and 3) inhibiting the viral replications. (Scheme 1) [19].

Previously there have been various physical and chemical modifications for NIC to improve its solubility; however, most of such studies were related to anti-cancer therapy. For example, poly ethylene glycol (PEG) was chemically conjugated with NIC in order to improve its bioavailability [12]. However, it is important to mention that there were

* Corresponding authors at: Intelligent NanoHybrid Materials Laboratory (INML), Institute of Tissue Regeneration Engineering (ITREN), Dankook University, Cheonan, 31116, Republic of Korea.

E-mail addresses: goeun.choi@dankook.ac.kr (G. Choi), jhchoy@dankook.ac.kr (J.-H. Choy).

<https://doi.org/10.1016/j.colsurfb.2021.112063>

Received 6 May 2021; Received in revised form 18 August 2021; Accepted 21 August 2021

Available online 24 August 2021

0927-7765/© 2021 Published by Elsevier B.V.

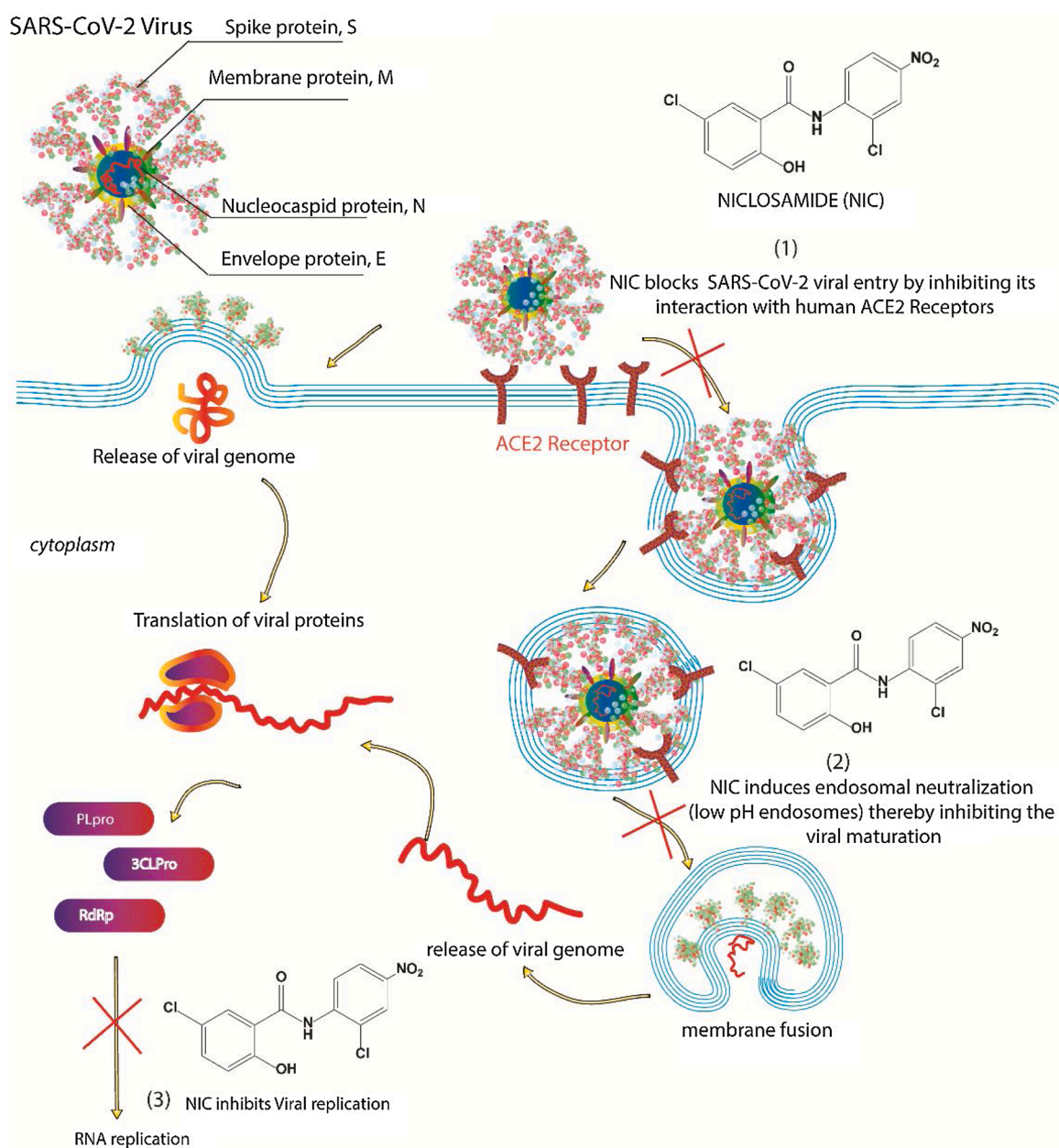
not so many published work related to injectable NIC formulations in the literature. In addition, most of the reported *in-vitro* experiments give a clarity neither on formulation nor on the NIC dissolving procedures.

In the present study, we formulated NIC with bovine serum albumin (BSA) and the resulting nanoparticles (NPs) were coated physically with PEG. The major reason for selecting BSA was due to its immense biocompatibility [20,21] and stabilizing capability [22]. Various biomedical applications including drug delivery [23–29], tissue engineering [30–33] and bio imaging, etc. extensively utilize BSA. It has also been reported that BSA modification could improve anti-viral potency [34] against Ebola pseudo viruses and virus like particles [35]. In addition, albumin plays a very important role in SARS-CoV-2 infection. Hypoalbuminemia, a condition, which is associated with severely affected COVID-19 patients and in such conditions, the virus can bind on serum albumin, dysregulating the cellular nutrient transportation and leading to systemic symptoms observed in SARS-CoV-2 infection and sepsis. When albumin bind to SARS-CoV-2 virions, this could lead to the

damage of endothelial glycocalyx by inhibition of albumin transport binding sites. This vascular endothelial glycocalyx (VEGLX) damage has also been reported as targeting regimen to treat COVID-19 [36]. In this context, rationally modified antiviral drug loaded serum albumin therapy might be beneficial for COVID-19 patients [37]. Additionally there have been several reports for hypoalbuminemia as an early diagnostic rational [38] and a targeting strategy towards COVID-19 [39].

On the other hand, PEGylation has been reported to improve the anti-viral effects [40], by enhancing the blood circulation of antiviral agents *in-vivo*. PEG has been extensively studied for drug delivery applications. Therefore, NIC would improve its therapeutic properties once they are modified with BSA and further coated with PEG for improved blood circulation, which might enhance their *in-vivo* efficacy [41].

In the present work, we are trying to address the following questions. 1) How effectively NIC molecules could be loaded into the BSA/PEG hybrids? 2) How nano-hybridization would affect the overall solubility of NIC? 3) What would be the future perspectives of these NIC-



Scheme 1. Anti-SARS-CoV-2 mechanism by Niclosamide (NIC): 1) Inhibition of endocytosis or autophagy; 2) enhanced endosomal neutralization and 3) Inhibition of viral replication inside the host cells. (PLpro-papain-like protease; 3CLPro-3CL like protease; RdRp-RNA dependent RNA polymerase).

Nanohybrids based on the *in-vivo* pharmacokinetics? The research hypotheses are as follows: 1) NIC being a neutral molecule, it could be stabilized using BSA via weak forces such as hydrogen bonding; 2) We expect that the solubility of NIC would be increased mainly because of the BSA stabilized structure of NIC; 3) We propose that PEG-BSA-Stabilized NIC NPs would be ideal in order to target SARS-CoV-2 for better efficacy either through extracellular or intracellular pathways (Scheme 1).

2. Materials and methods

2.1. Materials

NIC ($C_{13}H_8C_{12}N_2O_4$) was obtained from DERIVADOS QUIMICOS, Murcia, Spain. Anhydrous Ethanol (99.9%), and isopropyl alcohol (IPA) were purchased from Daejung, Gyeonggi-do, South Korea. BSA and (β -cyclodextrin) were purchased from Sigma Aldrich, USA. PEG, weight average molecular weight, $M_n \sim 10,000$, was purchased from Sigma, Milwaukee W1 53233, USA.

2.2. Synthesis of NIC NPs

For NIC NPs, 5 mg of NIC was dissolved in 1 mL IPA. Thus, prepared solution of $\sim 250 \mu\text{L}$ was directly added in to 9.75 mL of distilled water, where the particles were formed immediately with white opalescent coloration. The remnant IPA was evaporated by rotary evaporator (Heidolph Instruments Gm bH & Co. KG, 91126, Schwabach, Walpersdorfer Str. 12, Germany) for 15 min and the obtained solution was freeze-dried for 48 h.

2.3. Synthesis of BSA-NIC NPs

The PEG-BSA-NIC NPs were synthesized as follows; initially, NIC (5 mg/mL) was dissolved in IPA, from which 250 μL solution was drop wisely added in to 9.5 mL of distilled water containing BSA (50 mg/mL) until it formed an opalescent yellow coloration. Finally, 250 μL PEG (5 mg/mL) was added, followed by 15–30 min rotary evaporation to remove any remnant IPA. Detailed information is given in the Fig. S1.

2.4. Synthesis of PEG-BSA-NIC NPs

PEG-BSA-NIC NPs were synthesized as follows. Initially, NIC (5 mg/mL) was dissolved in IPA solution, from which 250 μL solution was drop wisely added in to 9.5 mL of distilled water containing BSA (50 mg/mL) until it formed an opalescent yellow coloration. Finally, 250 μL PEG (5 mg/mL) was added, followed by 15–30 min rotary evaporation to remove any remnant IPA. The resulting solution was freeze dried for 48 h in order to get the yellow powder, which was directly added in to 10 mL distilled water followed by probe sonication for 4 min. The uniform suspension was further syringe filtered using 0.45 μm PVDF filter (Fig. S2).

2.5. *In-vitro* release studies

The *in-vitro* drug release was done using dissolution apparatus. For the analysis, initially calibration curve was made in deionized water (DI water) (Fig. S3). In order to understand how NIC could be released from BSA-NIC and PEG-BSA-NIC NPs with and without serum conditions, two buffer solutions were made with a pH 7.4, of which one had 3% fetal bovine serum (FBS) added in it, mimicking the severe hypoalbuminemia condition (albumin < 2.5 g/dL) [42]. The pH of the dissolution media was chosen as 7.4 mainly because it mimics the blood pH [46]. 50 mg of samples were added in to ~ 310 mL solution in dissolution chamber. At pre-determined time intervals, 2.5 mL aliquots were withdrawn, and syringe filtered using 0.45 μm PVDF filters. The absorbance was measured at 340 nm using DI water as the solvent.

2.6. Stability studies

Stability studies were conducted at room temperature, refrigerator conditions (4 °C) and under serum condition (3%) respectively. The size and poly dispersity indices (PDI) were measured using Zeta Sizer (Otsuka Electronics DLS/Zeta EL-SZ-2000) for 3 weeks.

2.7. *In-vivo* pharmacokinetics

A pharmacokinetic (PK) study was performed in male Sprague-Dawley rats (7-week-old, 232–255 g). KNOTUS Co., Ltd. (Incheon, Korea) Institutional Animal Care and Use Committee (KNOTUS IACUC No. 20-KE-686) and Korea Conformity Laboratories (Incheon, Korea) IACUC (KCL IACUC No. approved the animal study IA20-03227). 2 mg/kg NIC in PEG-BSA-NIC NPs were injected intravenously single time. The NIC-nanohybrids were reconstituted in distilled water prior to the injection. In order to prepare for a control formulation, we made NIC solution using minimal additives. The two raw materials used to make NIC NPs are ethanol, which is a relatively bio-compatible solvent and the other is aqueous solution of β -cyclodextrin, which is widely used to dissolve hydrophobic drugs in water [43]. Accordingly, the control formulation was prepared by dissolving NIC in 0.24% β -cyclodextrin solution (ethanol-water mixture; 2:8 v/v) to make a final concentration of 2 mg/mL. The hydrodynamic size of the prepared NIC solution was less than 10 nm, implying that the NIC was well dissolved in the solution (Fig. 1). 2 mg/kg of control formulation was also injected intravenously to rats. Then the blood samples were collected by centrifuging for 2 min at 13,000 rpm in order to separate the plasma that was immediately frozen until further analysis using HPLC-mass spectrometry (HPLC-MS).

2.8. Quantification of NIC in rat's plasma

The blood ($\sim 600 \mu\text{L}$) was drawn from the jugular vein for analysis. A plasma calibration curve was prepared by using NIC standards at concentrations of 0, 5, 10, 50, 100, 500, 1000, and 2000 ng/mL. Samples were prepared by adding 100 μL of the internal standard, topiramate to 20 μL aliquot of rat plasma sample. In general, internal standard like topiramate drug is used to have a precise and accurate data, where volume errors are difficult to predict and control [44]. Then, they were vortexed for 5 s, followed by centrifugation at 13,000 g for 5 min at 4 °C. The 20 μL of supernatant was mixed with 180 μL of 50% methanol. Then, 150 μL of aliquot of the samples were transferred to sample vial for the analyses. Samples were analyzed by Acquity I-Class UPLC system (Waters) with mass spectrometer (Waters Xevo TQ-S). The LC analytical column was a Thermo Hypersil Gold (2.1 \times 50 mm, 1.9 μm) and was maintained at 50 °C during the measurements. Mobile phase was 5 mM ammonium acetate/water solution, and methanol with a flow rate of 0.4 mL/min.

2.9. Characterizations

The NMR analyses were conducted with Bruker/ Magnet System 500⁺54 Ascend at Dankook University Cheonan, South Korea, using D6-DMSO (Duetero.de, Sejong-si, 30128, South Korea) for all the experiments. The FT-IR studies were done with a Jasco FT-IR-6100 spectrometer (JASCO, Tokyo, Japan) using the standard KBr disk method in transmission mode (spectral range 4000–400 cm^{-1} , resolution 1 cm^{-1} , 40 scans per spectrum). For FT-IR, ~ 10 mg of samples were mixed with 100 mg of KBr pellet, ground properly by mortar and pestle. The obtained samples were pelletized under hydraulic press machine at 15–20 MPa for 1 min, which were then used for FT-IR characterization as described above. DLS and Zeta potential analyses were done using Otsuka Electronics DLS/Zeta EL-SZ-2000 (Japan) using disposable square cuvettes in distilled water, and serum containing distilled water as well. The concentration of the samples for DLS and Zeta was maintained to 10 mg/mL. UV Visible spectroscopy data were obtained using

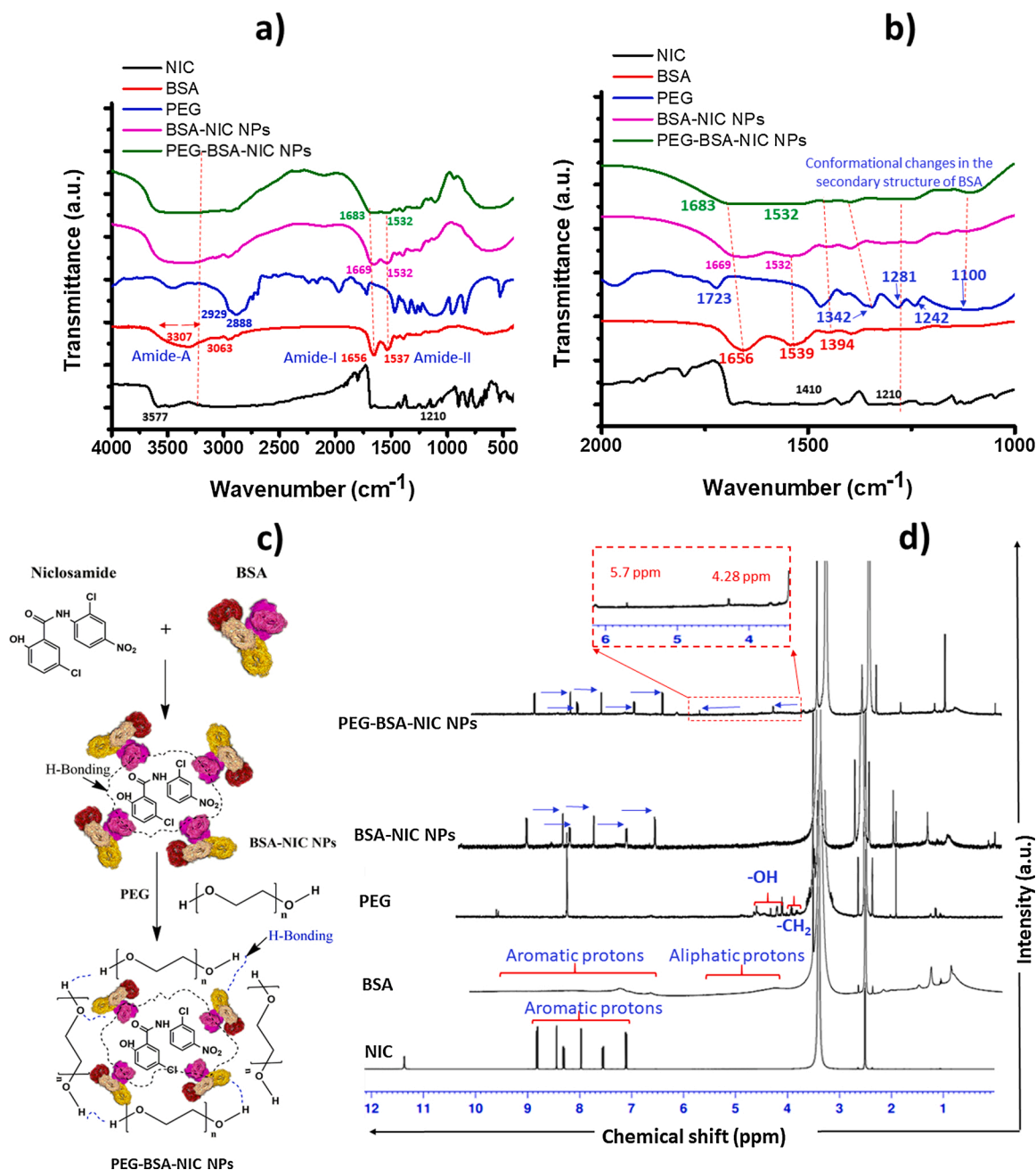


Fig. 1. Interaction of NIC within the developed soluble nanohybrids: a) full FT-IR spectra and b) carbonyl region-specific spectra of various samples such as control NIC, BSA, PEG, BSA-NIC NPs, and PEG-BSA-NIC NPs; c) proposed interaction of NIC with BSA, and PEG in the nanohybrids; d) proton NMR characterization for BSA, NIC, PEG, BSA-NIC NPs and PEG-BSA-NIC NPs respectively. The ← indicates the downfield whereas the → represents the upfield phenomenon in the samples.

JASCO-V630 Spectrophotometer (Easton, MA, USA), and the freeze-drying was carried out with ILSHIN BIOBASE (Gyeonggi-do, South Korea) South Korea) at -53°C . The field emission scanning electron microscopic (FE-SEM) analyses for various samples were done using a Sigma 300 (Carl Zeiss, Oberkochen, Germany) field-emission scanning electron microscope. The samples at a concentration of 1 mg/mL in distilled water were used for this. The prepared samples were dropped onto silicon wafer using 20 μL pipette and dried under ambient condition. Release studies were done using temperature controlled dissolution apparatus (DST-810 lab fine INC, Seoul, South Korea).

2.10. Statistical analysis

The statistical significances of the differences were evaluated with a

two-tailed Student's *t*-test. *P* value < 0.05 was considered as statistically significant.

3. Results

3.1. Synthesis and characterization of NIC-nanohybrids

NIC nanohybrids such as BSA-NIC NPs and PEG-BSA-NIC NPs were synthesised using a very simple co-acervation technique [45]. The interactions between NIC, BSA, and PEG were confirmed using FT-IR analyses. As shown in the Fig. 1, the characteristic peaks for NIC was found at 3577 and 1210 cm^{-1} respectively. These NIC characteristic peaks were assigned for $-\text{NH}$ stretching and $-\text{OH}$ in plane bending respectively. These two main peaks of NIC were absent in both BSA-NIC and

PEG-BSA-NIC NPs, possibly due to their involvement in hydrogen bonding interaction [46]. In addition, the methylene peak in the NIC was absent in both BSA-NIC and PEG-BSA-NIC NPs confirming that hydrogen bonding could be achieved through this functional group [47].

On the other hand, BSA stabilization of NIC was further confirmed by noticing the characteristic peak shifts compared to the control BSA alone. As per reported literature, BSA has characteristic peaks at ~ 1656 (Amide I, mostly due to the carbonyl (C=O) stretching vibration of the peptide linkages and stretching vibration bands of —OH groups), 1537 (Amide II, mostly from the in plane bending vibration of N—H and stretching vibrations of C—N bond), and ~ 3300 cm^{-1} , amide A (mostly stretching vibrations of —NH bond), respectively) [48]. It was noted that all the Amide-I and II bands were perturbed to either lower or higher wavelength (Fig. 1), indicating the changes in their secondary protein structure, owing to the well stabilization of NIC by BSA molecules as indicated in Fig. 1c.

PEG coating on BSA-NIC NPs was finally confirmed by observing the characteristic peak shifts of PEG bands. From the FTIR, it was clear that PEG had the characteristic bands at 2929 cm^{-1} , 2888 cm^{-1} , 1342 cm^{-1} , 1242 cm^{-1} and 1100 cm^{-1} respectively. The innate absorption peaks corresponding to the PEG such as C—O—C (antisymmetric stretching, 1342 cm^{-1}) with slight reduced intensities and complete disappearance of —OH characteristic peaks at 3455 cm^{-1} indicate a successful PEG coating on the BSA-NIC NPs. In addition, the C—OH peak at 1100 cm^{-1} was still retained in the FT-IR spectrum of PEG-BSA-NIC NPs indicating the possibilities of H-bonding with BSA-NIC NPs [49]. Similarly, C=O peak (1723 cm^{-1}) in the FTIR spectrum of PEG-BSA-NIC NPs was moved to lower range indicating its involvement in the H-bonding. In addition, the characteristic PEG peak around 2888 cm^{-1} corresponds to single bond CH_2 stretching vibration was completely vanished possibly due to the H-bonding with BSA-NIC NPs. As mentioned before, the specific band at 1110 cm^{-1} in both PEG and PEG coated BSA-NIC NPs remains unchanged indicating the presence of PEG surface coating. The band at 1281 cm^{-1} corresponds to C—O stretching vibration in PEG molecule, which was less intensified after coating with BSA-NIC NPs. The band at 1242 cm^{-1} in PEG corresponds to CH_2 twisting, and it has got less

intensified in PEG coated BSA-NIC NPs, possibly due to a hydrogen bonding [50].

Further, the FT-IR analyses were validated with the proton NMR data (Fig. 1d, the raw data are shown in supporting Fig. S4). After coating with BSA, the aromatic protons in the NIC were shifted indicating its participation in the H bonding. On the otherhand, the —NH proton in the NIC was shifted to upfield region from 11.4 to 9.0 ppm in the NMR spectrum of BSA-NIC NPs while PEG-BSA-NIC NPs had ~ 8.9 ppm respectively. In addition, the aromatic protons in NIC were upfield shifted after BSA and further PEG modification, clearly indicating that NIC molecules could be trapped within the BSA drug sockets. On the other hand, in BSA-NIC NPs, the aromatic protons corresponding to BSA molecules were downfield shifted indicating that there was a successful coating of BSA on the NIC NPs. Whereas, the PEG coating lead to downfield of its characteristic — CH_2 and —OH protons to higher ppm as indicated in the Fig. 1d. For example, the — CH_2 peaks originating from the repeat units of PEG, ie, — $(\text{CH}_2\text{CH}_2\text{O})_n$, at ~ 3.7 – 3.9 ppm and —OH peaks (4.1 – 4.6 ppm) were downfield shifted 4.28 and 5.7 respectively [51,52]. This clearly indicating that PEG molecules can be coated on the surface of BSA-NIC NPs via a strong hydrogen bonding interaction. The aromatic protons in BSA were additionally upfield in the NMR spectrum of PEG-BSA-NIC NPs, indicating the possibility of well coated PEG molecules on its surface.

3.2. Particle size and FE-SEM analyses

The DLS analyses showed that both BSA-NIC and PEG-BSA-NIC NPs had optimum size in the range of <150 nm. However, after PEG coating, BSA-NIC NPs reduced significantly low particle size from 153 ± 2.61 – 110 ± 3.67 nm (Fig. 2a, b). This might be due to the PEG coating, wherein it can well stabilize the particle. In fact, it is well known that PEG coating can reduce the particle size mainly due to its capping nature. Thanks to the hydroxyl groups in PEG which can reduce the agglomeration via capping effect [53,54]. On the other hand, the β -cyclodextrin NIC nano formulation had shown ultra small particle size (Fig. S5).

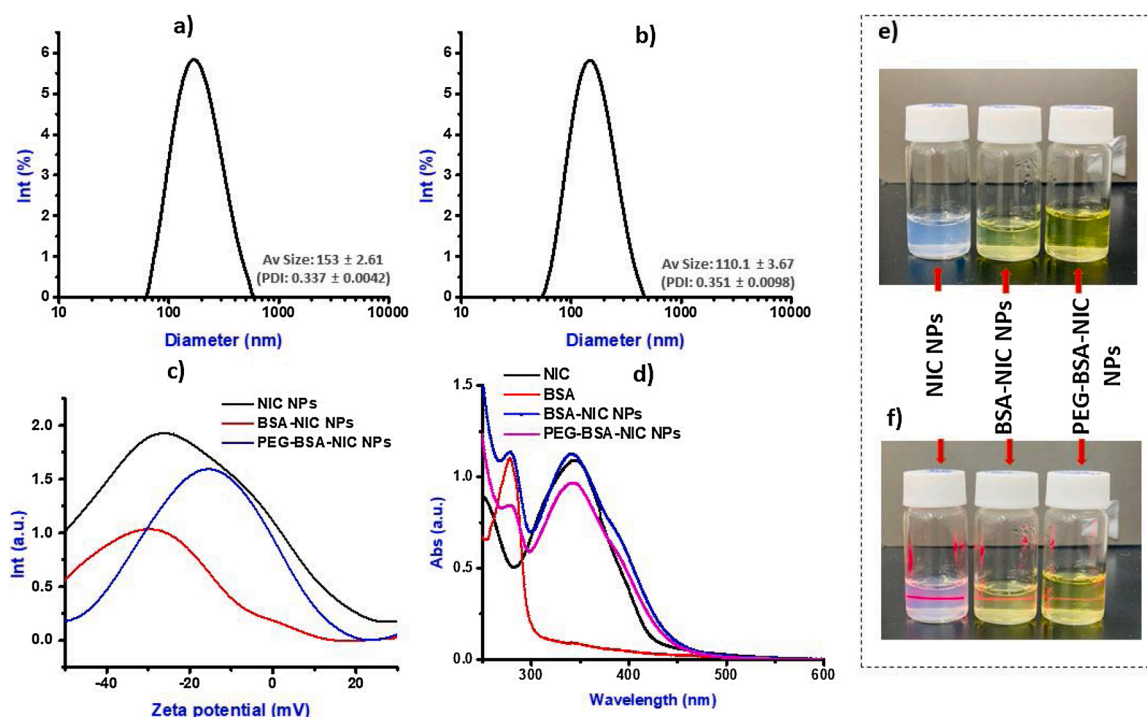


Fig. 2. Particle size analysis by DLS: a) BSA-NIC NPs; b) PEG-BSA-NIC NPs; and c) zeta potential and d) UV analysis and e) & f) shows colloidal stability of various samples such as NIC NPs, BSA-NIC NPs, and PEG-BSA-NIC NPs respectively. (e-without laser and f-with laser-Tyndall effect).

The zeta potential for control NIC NPs was found to be around -27.03 ± 3.69 mV, whereas the BSA-NIC NPs showed almost similar zeta potential as that of control NIC NPs (-32.19 ± 1.39 mV). This could be mainly because of the interaction between NIC and BSA, indicating that either BSA must have coated on the surface or NIC could be get inside the drug sockets of BSA. On the other hand, PEG coating on the BSA-NIC NPs shifted the zeta potential significantly towards a lower values (-16.55 ± 0.75 mV) (Fig. 2c). This indicated a proper coating of PEG on the surface of BSA-NIC NPs. All the NPs were stable right after they were prepared freshly, as shown in the Fig. 2e with a good Tyndall effect on laser exposure (Fig. 2f).

Further, UV analysis was done on various samples including NIC, BSA-NIC and PEG-BSA-NIC NPs in order to understand whether there was any characteristic peak shift for NIC, before and after modification with BSA, and PEG. UV spectra showed a major characteristic band for BSA at 277 nm, originated from the aromatic amino acids (Trp, Tyr, and Phe) and backbone ($n \rightarrow \pi^*$ transition, peptide bond) of BSA. NIC showed its characteristic peak at ~ 345.5 nm in water, whereas, BSA showed its specific peak at 277 nm. On modification with BSA, the BSA-NIC hybrids were able to maintain their individual peaks at 279 (BSA) and 340 nm (NIC). The slight blue shift of NIC absorption from 340 to 345.5 nm indicated their encapsulation in the BSA (Fig. 2d). Similarly, the NIC peak (340 nm) was blue shifted to 342 in PEG-BSA-NIC NPs as well. Moreover, the BSA bands were slightly shifted on modification with BSA and PEG (Fig. S6), indicating their secondary bonding might have affected on NIC loading through H-bonding.

It should be noted that BSA is globulin molecule having large molecular size with loose structure, entailing its hydrophobic cavities for drug loading or encapsulation. When poorly water-soluble NIC molecules were added, BSA could interact with NIC through the hydrogen bonding, resulting in compact molecular self-assembled structure. On the other hand, when NIC molecules get into the drug sockets of BSA, its total conformation would have changed. This protein-disrupted structure of BSA suggests that the conformation of BSA might have changed through a strong interaction between BSA and NIC [55].

Further, we analyzed the morphology of developed BSA-NIC and PEG-BSA-NIC NPs by FE-SEM. The particle size obtained from DLS measurements were almost matched with the FE-SEM results shown in the supporting Fig. S7 with very small average particle size. The rod shaped morphology could be due to a thermodynamically more stable structure of the PEG-BSA-NIC NPs [56]. The elongated NIC structures (Fig. S7a) were cut down into smaller pieces of <150 nm, indicating that BSA and PEG modification would enhance their solubility for better *in-vitro* and *in-vivo* therapeutic outcome. It should also be noted that SARS-CoV-2 viral particles were reported to possess a size <100 nm. Therefore, in order to adsorb such small sized virions, it is important to

match with their size in the optimum range. We expect that our rod shaped, PEG-BSA-NIC NPs might be a good strategy in this context. In addition, the rod shaped NPs reported to possess better blood circulation than the spherical NPs [57].

3.3. *In-vitro* solubility and stability

The major problem associated with NIC has been its solubility. Therefore, our most important priority was to improve its solubility by modifying with BSA and PEG moieties. Here, compared to the NIC NPs alone, the powdered BSA-NIC NPs and PEG-BSA-NIC NPs were readily solubilized in water as shown in the Fig. 3. In addition, a real time video footage was given in the supporting information as Video S1 (<https://drive.google.com/file/d/1pRcZUSQobEPQZiPeZ7kFXSjMUNCqu8zp/view?usp=sharing>) and Video S2 (https://drive.google.com/file/d/1_w25HSD-lwiPH2zSCGZo8cwrFVvesfgr/view?usp=sharing), which clearly shows the readily water soluble characteristic property after modifying with BSA and PEG.

Further, we have checked a long-term stability of NIC-nanohybrids at three different conditions such as room temperature (RT), refrigerator (4°C) and with 3 % serum. As observed in the Fig. 4, both BSA-NIC and PEG-BSA-NIC NPs could retain the particle size pretty well over 3 weeks. Whereas the NIC-NPs showed irregular size as per DLS along with very high poly dispersity indices (Fig. S8). It is worthy to mention that even after 3 weeks, all the samples showed very good stability in terms of PDI (poly dispersity index) and Tyndall effect as shown in Supporting Figs. S8 and 9.

However, the particle size for the NIC NPs were unstable especially in the room temperature and refrigerator conditions after two weeks whereas, in the serum conditions they were stable, with large particle size (<500 nm). In addition, the PDI values for control NIC NPs were irregular indicating that they could be destabilized in the solution form, necessitating a proper coating, as we demonstrated in the present study. On the other hand, even though, both BSA-NIC and PEG-BSA-NIC NPs were stable at three different conditions as mentioned, the particle size seemed increasing from week 1. Therefore, it is advised to store the formulation as a freeze-dried powdered form rather than in a solution form. In a clinical aspect, therefore, we recommend to keep these formulations in powder samples until it can be reconstituted in the desirable intravenously injectable solution (IV solution).

3.4. *In-vitro* drug release studies

Table S1 shows the details of NIC contents in various injectable samples. After understanding the drug contents, we conducted *in-vitro* drug release studies using two samples such as BSA-NIC NPs and PEG-

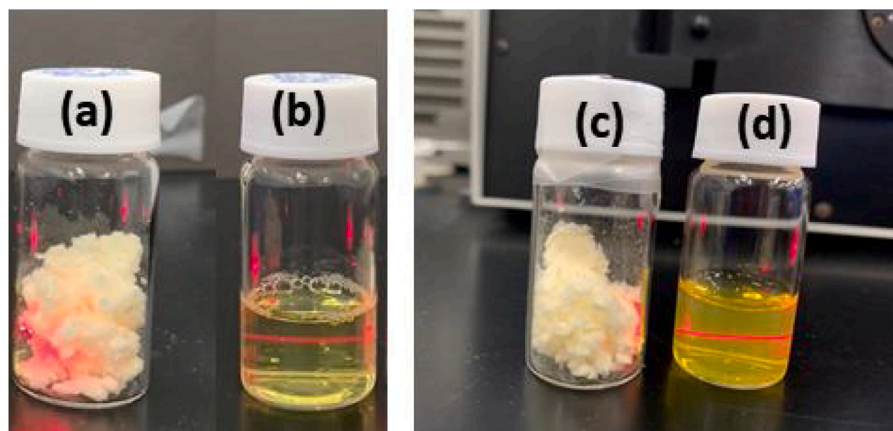


Fig. 3. Readily water soluble NIC-Nanohybrids. a) Lyophilized powder form for BSA-NIC NPs after 48 h, b) its readily soluble form in water; c) lyophilized powder form for PEG-BSA-NIC NPs after 48 h and d) its representative image showing readily soluble characteristics in water.

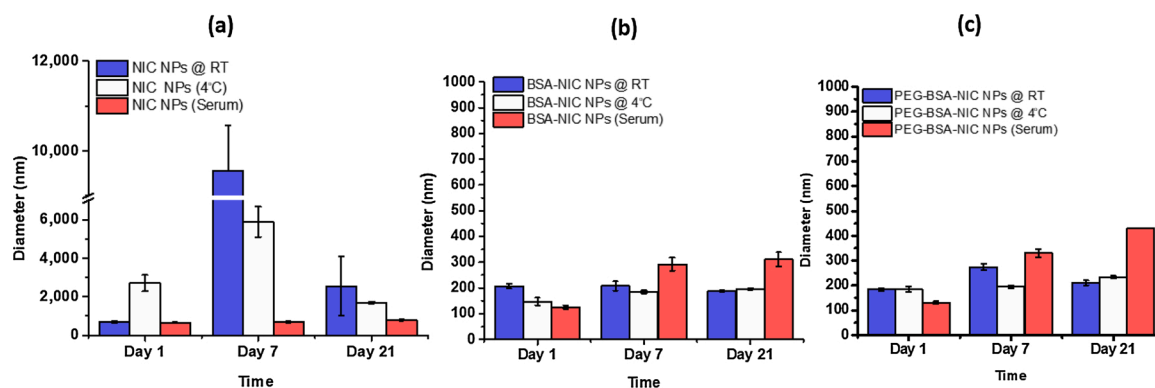


Fig. 4. *In-vitro* stability of NIC and its nanohybrid formulations by particle size variation in DLS. a) NIC NPs; b) BSA-NIC NPs and c) PEG-BSA-NIC NPs under room temperature, 4 °C and serum conditions from day 1 to 21 ($n = 3$).

BSA-NIC NPs with two different ratios such as 2:5 and 1:40 (NIC:BSA ratio). These two formulations with different concentrations of BSA were tested in order to understand how BSA concentration would account for the drug release pattern. As shown in Fig. 5, it was obvious that both NPs were stable in serum conditions and thereby better release pattern under serum conditions than that at non-serum buffer (pH 7.4). It was noted that the BSA concentration had slightly improved the release pattern under serum conditions (Fig. 5b). This might be attributed for the high stability of NIC hybrids with higher amount of BSA,

which was further improved under serum conditions. Approximately ~80 % NIC was released under the serum conditions from 1:40 ratio sample with PEG coating, indicating that NIC molecules could be better solubilized in the presence of BSA and PEG. Previously there have been such reports for better drug release profile by BSA stabilization [58]. In addition, BSA [59] as well as PEG modified NPs [60] can show a controlled release pattern as well.

3.5. *In-vivo* pharmacokinetics

Finally, the as made PEG-BSA-NIC NPs were tested for *in-vivo* bioavailability using rats. The samples were injected into female Sprague-Dawley rats at 2 mg/kg as mentioned previously. Fig. 6 represents the plasma concentration-time profiles for NIC from PEG-BSA-NIC NPs and control NIC formulation. From the PK data, it was very clear that, the C_{max} could be attained in the plasma very quickly in 15 min. Obviously the rapid absorption might be due to the direct delivery of NIC in the blood stream. This systemic circulation almost instantaneously sustained until 6 h though the NIC concentrations were retained below 50–100 ng/mL. Compared with the PK profile of control formulation, NIC (dissolved in organic solvent), PEG-BSA-NIC NPs seemed helping to maintain the NIC concentration in blood for a long time.

On the other hand, the control NIC formulation cleared very quickly

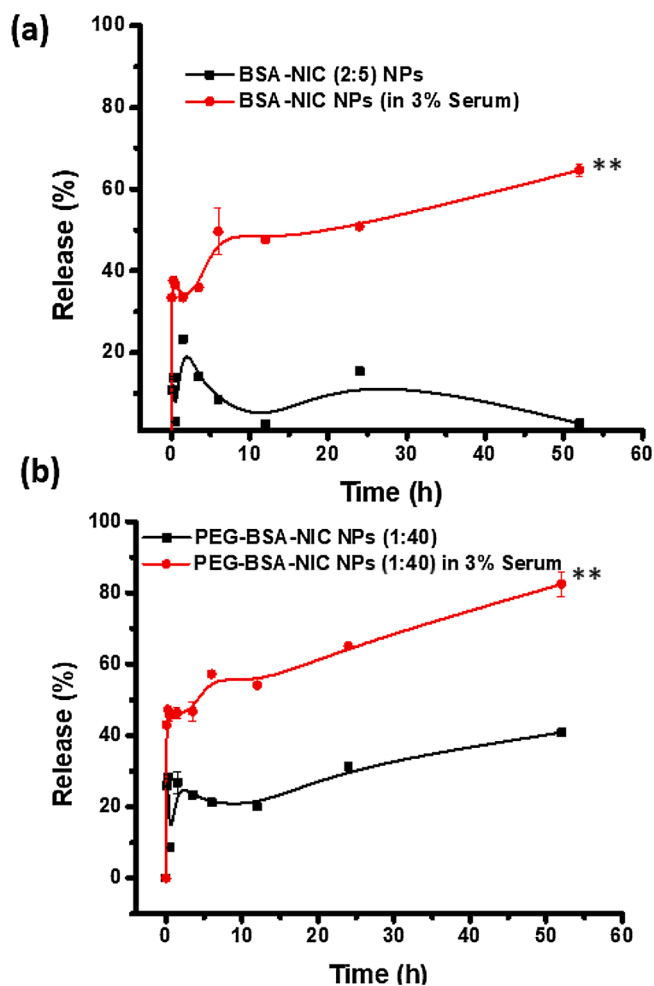


Fig. 5. *In-vitro* NIC release under serum and non-serum conditions using pH 7.4 solutions. a) BSA-NIC (2:5) NPs and b) PEG-BSA-NIC NPs (1:40) respectively ($n = 3$, $**p < 0.05$).

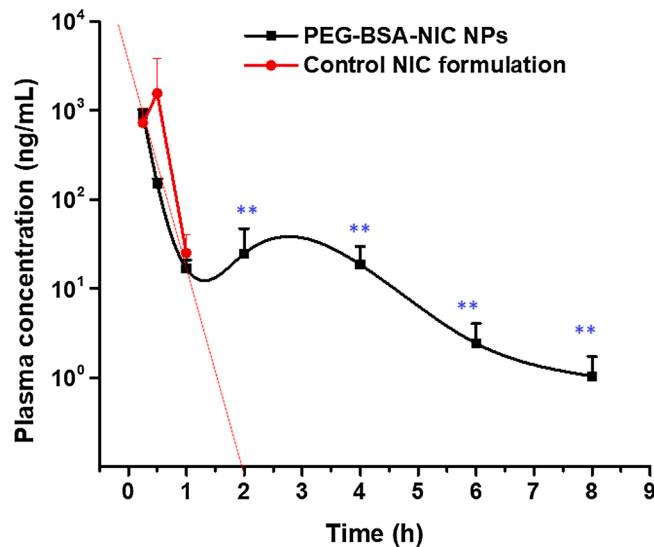


Fig. 6. *In-vivo* plasma concentrations of NIC followed by a single administration of intravenous injection (2 mg/kg) in rats from PEG-NIC-BSA NPs and NIC control formulation respectively.

from the body within 2 h indicating the poor stability thereby low absorption of NIC than the PEG-BSA-NIC NPs. The sustained circulation until 6 h could be due to the physical coating of PEG molecules. It is well known that PEG modification could effectively improve the blood circulation by inhibiting the opsonin adhesion, thereby escaping the phagocytic capture [61].

As shown in Fig. 6, the mean area under the concentration-time curve (AUC-last) was calculated to be 375.49 ± 63.27 (ng h/mL). The detailed PK parameters were given in the Table 1.

Table 1, shows that PEG-BSA-NIC NPs were able to maintain the plasma concentration of NIC quite longer time in comparison with the control NIC formulation. Though the AUC was slightly higher for the β -cyclodextrin-NIC control formulation, their $t_{1/2}$ was very low and therapeutically irrelevant. On the other hand, it is worthy to say that PEG-BSA-NIC NPs could improve almost ~ 8.35 fold higher $t_{1/2}$ than the control NIC formulation. The AUC value for control NIC formulation was quite higher 552.40 ± 303.76 ng·h/mL, while they showed very low $t_{1/2}$ (0.15 ± 0.02 h). On the other hand, the both PEG-BSA-NIC NPs and β -cyclodextrin-NIC control formulation exhibited same t_{max} of 0.25 h with high C_{max} for the PEG-BSA-NIC NPs (904.76 ± 117.52 ng/mL). It should be noted that a maximum NIC concentration from PEG-BSA-NIC NPs was achieved in a sustained manner as the $t_{1/2}$ was very high (1.28 ± 0.41 h). This sustained plasma NIC concentration might be beneficial for achieving better anti-COVID therapeutic outcome than the control sample.

4. Discussion

The present pandemic situation is an emergency as the daily COVID-19 cases are surging worldwide under the 4th wave. Despite of the worldwide vaccination strategies, where it can only prevent the diseases, there are millions still suffering with COVID-19, especially with the newly mutated delta [62–64] and lambda variants. In particular, old aged group with existing health issues such as diabetes and cardiovascular diseases are vulnerable. Therefore, a proper anti-COVID-19 therapeutic strategy is of great scope. However, finding a completely new medication has always been a challenge. On the other hand, there have been several potential drug candidates, with negligible bio-availability owing to their poor water solubility. The present drug candidate, NIC, in our study is such a candidate. Here our main challenge is to improve NIC solubility and eventually achieve anti-viral effects.

Firstly, the major reason for choosing BSA was to improve the drug solubility of NIC. Previously, Chen et al. (2018) reported stabilization of poorly water soluble curcumin by BSA [65]. Secondly, to utilize BSA as a specific targeting agent for the infected sites under hypoalbuminemia condition due to the SARS-CoV-2, which has been well reported, particularly in severely affected patients [66]. For example, Huang et al. (2020) found that hypoalbuminemia could result in poor prognosis in COVID-19 patients [67].

In this aspect, BSA itself could be selectively taken up by the infected cells. Hypoalbuminemia majorly observed in patient with diabetes [68] and cardiovascular diseases [69], and these groups are highly prone to

COVID-19, leading to mortality. Hypoalbuminemia condition leads to a poor prognosis in 80 % of the non-surviving COVID-19 positive patients. This could be due to the fact that serum albumin maintains plasma oncotic pressure and function as a vehicle for different endogenous/exogenous compounds. Even though hypoalbuminemia is not considered as a cause of underlying pathology, it is more like a condition, therefore, albumin based strategical therapeutic approaches would be highly advantageous for COVID-19.

In the present study, it was very clear that poorly soluble NIC drug was able to be readily water-soluble after albumin coating, and PEGylation, indicating its successful i.v. formulation, for the first time (Video S1 & S2). However, in the previously reported oral formulation (200 mg/kg) for anti-cancer therapy, the *in-vivo* PK performance was determined to be below 100 ng/mL [70]. In fact we achieved almost the similar PK profile with the readily water-soluble i.v. formulation at the 2 mg/kg dosage, and therefore, this might be advantageous to have better anti-COVID outcome in clinical model.

Another highlight in our case was the smaller particle size < 150 nm, particularly for the PEG-BSA-NIC NPs, and this could be beneficial for easy adsorption on the virus with similar size, thereby better internalization within the host cells. The SARS-CoV-2 has less than 200 nm particle size [71]. The comparatively low availability of our intravenously injected PEG-BSA-NIC NPs might be associated with non-hypoalbuminemia condition in the normal rats.

It should be noted that, injectable formulations were hardly explored for NIC. The major studies reported were PEG covalently modified with NIC, which was developed for cancer therapy to treat SKOV-3 tumor xenograft in NOD/SCID mouse [72]. Even though, their PK studies showed less than 50–100 ng/mL of NIC plasma concentration, the NIC formulation (by electro spraying) was able to induce antitumor efficacy in SKOV-3 xenograft model indicating that, the present PEG-BSA-NIC NPs might be therapeutically beneficial for viral infected cells too.

In many of the reported studies related to screening FDA approved drug candidates for SARS-CoV-2 virus, the methodology related to drug formulation was not mentioned clearly (Fig. S10). In that context, a readily water/biological fluid (Culture media) soluble NIC formulation is of great relevance.

In the future studies, we will be analyzing how these readily soluble NIC nanohybrids could target the SARS-CoV-2 infected sites under hypoalbuminemia condition? We hypothesize that a damaged glyco-calyx could lead to hypoalbuminemia condition there by higher chance of cellular intake of albumin coated NPs. In addition, we hypothesize that when albumin coated NIC nanohybrids bind with the viral particles, it could easily enter the infected cells allowing intra cellular anti-viral mechanism.

Under an injury or sepsis condition associated with COVID-19, glyco-calyx damage was reported to be dominant, meaning that viral particles could easily get into host cells as the barrier is already damaged. In addition, the hypoalbuminemia condition could lead to an enhanced cellular uptake of serum albumin coated NIC nanohybrids. Our future studies on the present nanohybrids will be oriented on this aspect with the SARS-CoV-2 infected model (Scheme S1).

5. Conclusions

We successfully developed highly water soluble and injectable PEG-BSA-NIC NPs, having optimum particle size < 150 nm. The *in-vitro* characterizations such as FT-IR, NMR, DLS and zeta analyses clearly showed the successful PEG coating on BSA-NIC NPs. The present injectable formulations were stable for 3 weeks under ambient condition at room temperature and at 4 °C in refrigerator, and in serum. Further, the *in-vitro* NIC release from PEG-BSA-NIC NPs was significantly higher even in the serum condition. Compared to the previous studies related to intraperitoneal NIC formulation [12], we were able to make an i.v. one, for the first time, which was readily water soluble, resulting in improved bioavailability. In addition, the average particle size of PEG-BSA-NIC

Table 1

PK parameters of PEG-BSA-NIC NPs and control NIC formulation after a single intravenous administration into rats.

PK parameters	PEG-BSA-NIC NPs	Control cyclodextrin-NIC NPs
*AUC (last) (ng h/mL)	375.49 ± 63.27	552.40 ± 303.76
*AUC(<i>Infinite</i>) (ng h/mL)	378.18 ± 62.98	565.07 ± 311.07
** C_{max} (ng/mL)	904.76 ± 117.52	723.67 ± 345.83
*** t_{max} (h)	0.25 ± 0.00	0.25 ± 0.00
**** $t_{1/2}$ (h)	1.28 ± 0.41	0.15 ± 0.02

* AUC- Area under the curve.

** C_{max} - maximum plasma concentration.

*** t_{max} -time required to reach C_{max} .

**** $t_{1/2}$ - elimination half-life.

NPs lower than 150 nm, as determined by the DLS method (Fig. 2), could be considered as an ideal one for injectable solution. Their thickness could also be estimated from the SEM study (~20 nm in diameter in Fig. S7), which was significantly smaller than the previous reports on the NIC formulation with a size of ~100 nm in diameter and ~500 nm in length [72]. According to the PK studies for the present PEG-BSA-NIC nanohybrid drug and the control NIC formulation, the plasma concentration of NIC for the former was determined to be less than 100 ng/mL, whereas its $t_{1/2}$ value was greatly improved to be 1.28 h, which was ~8.35 fold higher than that of the latter, the control NIC (0.15 h). In such a way the NIC concentration could be well sustained in the systemic circulation and would be useful for treating COVID-19. We still believe that our readily water-soluble NIC nanohybrids would be very effective in clinical model of SARS-CoV-2 virus and we are on the way to understand how these NIC nanohybrids would enhance the therapeutic outcome in a hypoalbuminemia model sooner.

CRedit authorship contribution statement

N. Sanoj Rejinold: Methodology, Investigation, Writing - original draft, Writing - review & editing. **Huiyan Piao:** Investigation. **Geunwoo Jin:** Investigation, Writing - review & editing. **Goeun Choi:** Investigation, Writing - review & editing, Project administration, Funding acquisition. **Jin-Ho Choy:** Conceptualization, Investigation, Supervision, Writing - review & editing, Project administration, Funding acquisition.

Declaration of Competing Interest

The authors declare that they have no known competing financial interests or personal relationships that could have appeared to influence the work reported in this paper.

Acknowledgements

This research was supported by Basic Science Research Program through the National Research Foundation of Korea (NRF) funded by the Ministry of Education (No. 2020R111A2074844), by the NRF grant funded by the Korea government (MSIT) (No. 2020R1F1A1075509), and under the framework of the International Cooperation Program managed by NRF (No. 2017K2A9A2A10013104).

Appendix A. Supplementary data

Supplementary data associated with this article can be found, in the online version, at <https://doi.org/10.1016/j.colsurfb.2021.112063>.

References

- [1] J. Wise, Covid-19: new coronavirus variant is identified in UK, *BMJ-Br. Med. J.* 371 (2020).
- [2] A. Rezagholizadeh, S. Khiali, P. Sarbakhsh, T. Entezari-Maleki, Remdesivir for treatment of COVID-19; an updated systematic review and meta-analysis, *Eur. J. Pharmacol.* 897 (2021).
- [3] V.V. Tkach, M.V. Kushnir, S.C. de Oliveira, Y.G. Ivanushko, A.V. Velyka, A. F. Molodiantu, P.I. Yagodynets, Z.O. Kormosh, L.V. dos Reis, O.V. Luganska, K. V. Palamarek, Y.L. Bredikhina, Theoretical description for anti-COVID-19 drug Remdesivir electrochemical determination, assisted by squaraine dye-Ag2O2 composite, *Biointerface Res. Appl.* 11 (2021) 9201–9208.
- [4] V.C. Yan, F.L. Muller, Remdesivir for COVID-19: why not dose higher? *Antimicrob. Agents Chemother.* 65 (2021).
- [5] K. Juneja, R. Humeniuk, D. Porter, H.Y. Cao, J. Feng, Reply to Yan and Muller, "Remdesivir for COVID-19: why not dose higher?", *Antimicrob. Agents Chemother.* 65 (2021).
- [6] Y. Shen, W. Eades, B.F. Yan, Remdesivir potently inhibits carboxylesterase-2 through covalent modifications: signifying strong drug-drug interactions, *Fund Clin. Pharmacol.* 35 (2021) 432–434.
- [7] B.T. Garibaldi, K.B. Wang, M.L. Robinson, S.L. Zeger, K. Bandeen-Roche, M. C. Wang, G.C. Alexander, A. Gupta, R. Bollinger, Y.X. Xu, Comparison of time to clinical improvement with vs without Remdesivir treatment in hospitalized patients with COVID-19, *JAMA Network Open* 4 (2021).
- [8] Y.C. Xie, X.Z. Guo, T.W. Hu, D.B. Wei, X.L. Ma, J.Q. Wu, B. Huang, J.S. Shen, Significant inhibition of porcine epidemic diarrhea virus in vitro by Remdesivir, its parent nucleoside and beta-d-N-4-hydroxycytidine, *Virology* (2021) 1–9, <https://doi.org/10.1007/s12250-021-00362-2>.
- [9] O. Dyer, Covid-19: Remdesivir has little or no impact on survival, WHO trial shows, *BMJ* 371 (2020) m4057.
- [10] M.O. Jara, Z.N. Warnken, R.O. Williams, Amorphous solid dispersions and the contribution of nanoparticles to in vitro dissolution and in vivo testing: niclosamide as a case study, *Pharmaceutics* 13 (2021).
- [11] A. Mostafa, A. Kandeil, Y.A.M.M. Elshaiar, O. Kutkat, Y. Moatasim, A.A. Rashad, M. Shehata, M.R. Gomaa, N. Mahrous, S.H. Mahmoud, M. GabAllah, H. Abbas, A. El Taweel, A.E. Kayed, M.N. Kamel, M. El Sayes, D.B. Mahmoud, R. El-Shesheny, G. Kayali, M.A. Ali, FDA-approved drugs with potent in vitro antiviral activity against severe acute respiratory syndrome coronavirus 2, *Pharmaceutics* 13 (2020).
- [12] R. Ma, Z.G. Ma, J.L. Gao, Y. Tai, L.J. Li, H.B. Zhu, L. Li, D.L. Dong, Z.J. Sun, Injectable pegylated niclosamide (polyethylene glycol-modified niclosamide) for cancer therapy, *J. Biomed. Mater. Res. Part A* 108 (2020) 30–38.
- [13] J.J. Liu, Niclosamide reverses cisplatin resistance by inhibiting Bcl-2 and Stat3 in HER2-positive breast cancer, *Cancer Res.* 81 (2021).
- [14] Sauraj, A. Kumar, B. Kumar, A. Kulshreshtha, Y.S. Negi, Redox-sensitive nanoparticles based on xylan-lipoic acid conjugate for tumor targeted drug delivery of niclosamide in cancer therapy, *Carbohydr. Res.* 499 (2021) 108222.
- [15] M.C. Huang, Q. Qiu, S. Zeng, Y.J. Xiao, M.H. Shi, Y.Y. Zou, Y.J. Ye, L.Q. Liang, X. Y. Yang, H.S. Xu, Niclosamide inhibits the inflammatory and angiogenic activation of human umbilical vein endothelial cells, *Inflamm. Res.* 64 (2015) 1023–1032.
- [16] W. Chen, R.A. Mook, R.T. Premont, J.B. Wang, Niclosamide: beyond an antihelminthic drug, *Cell. Signal.* 41 (2017) 89–96.
- [17] N.C. Gassen, D. Niemeier, D. Muth, V.M. Corman, S. Martinelli, A. Gassen, K. Hafner, J. Papies, K. Mösbauer, A. Zellner, A.S. Zannas, A. Herrmann, F. Holsboer, R. Brack-Werner, M. Boshart, B. Müller-Myhsock, C. Drosten, M. A. Müller, T. Rein, SKP2 attenuates autophagy through Beclin1-ubiquitination and its inhibition reduces MERS-Coronavirus infection, *Nat. Commun.* 10 (2019) 5770.
- [18] C.J. Wu, J.T. Jan, C.M. Chen, H.P. Hsieh, D.R. Hwang, H.W. Liu, C.Y. Liu, H. W. Huang, S.C. Chen, C.F. Hong, R.K. Lin, Y.S. Chao, J.T.A. Hsu, Inhibition of severe acute respiratory syndrome coronavirus replication by niclosamide, *Antimicrob. Agents Chemother.* 48 (2004) 2693–2696.
- [19] S.K.S.S. Pindiprolu, S.H. Pindiprolu, Plausible mechanisms of Niclosamide as an antiviral agent against COVID-19, *Med. Hypotheses* 140 (2020).
- [20] K. Areevijit, N. Dhanesuan, J.A. Luckanagul, S. Rungsianont, Biocompatibility study of modified injectable hyaluronic acid hydrogel with mannitol/BSA to alveolar bone cells, *J. Biomater. Appl.* 35 (10) (2021) 1294–1303.
- [21] J. Wang, L.Y. Cui, Y.D. Ren, Y.H. Zou, J.L. Ma, C.J. Wang, Z.Y. Zheng, X.B. Chen, R. C. Zeng, Y.F. Zheng, In vitro and in vivo biodegradation and biocompatibility of an MMT/BSA composite coating upon magnesium alloy AZ31, *J. Mater. Sci. Technol.* 47 (2020) 52–67.
- [22] M. Saito, L.-J. Yin, I. Kobayashi, M. Nakajima, Comparison of stability of bovine serum albumin-stabilized emulsions prepared by microchannel emulsification and homogenization, *Food Hydrocoll.* 20 (2006) 1020–1028.
- [23] P.U. Maheswari, R. Muthappa, B.K. Purushothaman, K.M.M.S. Begum, Evaluation of folic acid functionalized BSA-CaFe(2)O(4)nanohybrid carrier for the controlled delivery of natural cytotoxic drugs hesperidin and eugenol, *J. Drug Deliv. Sci. Technol.* 61 (2021).
- [24] M.R.F. Mazzilli, J.A.R. Ambrosio, D.D. Godoy, A.D. Abreu, J.A. Carvalho, M. Beltrame, A.R. Simioni, Polyelectrolytic BSA nanoparticles containing silicon dihydroxide phthalocyanine as a promising candidate for drug delivery systems for anticancer photodynamic therapy, *J. Biomater. Sci. Polym. E* 31 (2020) 1457–1474.
- [25] N. Sedyakina, A. Kuskov, K. Velonia, N. Feldman, S. Lutsenko, G. Avramenko, Modulation of entrapment efficiency and in vitro release properties of BSA-loaded chitosan microparticles cross-linked with citric acid as a potential protein-drug delivery system, *Materials* 13 (2020).
- [26] D.P. Damera, S. Kaja, L.S.L. Janardhanam, S. Alim, V.V.K. Venuganti, A. Nag, Synthesis, detailed characterization, and dual drug delivery application of BSA loaded aquasomes, *ACS Appl. Bio Mater.* 2 (2019) 4471–4484.
- [27] J.N. Lu, Q.W. Chen, X.C. Ding, J. Wen, Y.H. Zhang, H.J. Li, Y.Q. Xu, F.Y. Liu, S. S. Chen, S.G. Sun, BSA modified, disulfide-bridged mesoporous silica with low biotoxicity for dual-responsive drug delivery, *Microporous Mesoporous Mater.* 278 (2019) 257–266.
- [28] C. Fu, C.Z. Ding, X.C. Sun, A.L. Fu, Curcumin nanocapsules stabilized by bovine serum albumin-capped gold nanoclusters (BSA-AuNCs) for drug delivery and theranosis, *Mater. Sci. Eng. C-Mater.* 87 (2018) 149–154.
- [29] H. Shagholani, S.M. Ghoreishi, S.H. Sharifi, Conversion of amine groups on chitosan-coated SPIONs into carbocyclic acid and investigation of its interaction with BSA in drug delivery systems, *J. Drug Deliv. Sci. Technol.* 45 (2018) 373–377.
- [30] T.X. Li, L. Wang, Y.F. Huang, B.J. Xin, S. Liu, BSA loaded bead-on-string nanofiber scaffold with core-shell structure applied in tissue engineering, *J. Biomater. Sci. Polym. E* 31 (2020) 1223–1236.
- [31] L. Xing, J.C. Sun, H.P. Tan, G.L. Yuan, J.L. Li, Y. Jia, D.S. Xiong, G. Chen, J.Z. Lai, Z.H. Ling, Y. Chen, X.H. Niu, Covalently polysaccharide-based alginate/chitosan hydrogel embedded alginate microspheres for BSA encapsulation and soft tissue engineering, *Int. J. Biol. Macromol.* 127 (2019) 340–348.
- [32] T.X. Li, X. Ding, L.L. Tian, S. Ramakrishna, Engineering BSA-dextran particles encapsulated bead-on-string nanofiber scaffold for tissue engineering applications, *J. Mater. Sci.* 52 (2017) 10661–10672.

- [33] R.A. Bakare, C. Bhan, D. Raghavan, Synthesis and characterization of collagen grafted poly(hydroxybutyrate-valerate) (PHBV) scaffold for loading of bovine serum albumin capped silver (Ag/BSA) nanoparticles in the potential use of tissue engineering application, *Biomacromolecules* 15 (2014) 423–435.
- [34] A. Arnedo, J.M. Irache, G. González Gaitano, M. Valgañón, S. Espuelas, Bovine serum albumin modified the intracellular distribution and improved the antiviral activity of an oligonucleotide, *J. Drug Target.* 11 (2003) 197–204.
- [35] H. Li, F. Yu, S. Xia, Y. Yu, Q. Wang, M. Lv, Y. Wang, S. Jiang, L. Lu, Chemically modified human serum albumin potentially blocks entry of Ebola pseudoviruses and viruslike particles, *Antimicrob. Agents Chemother.* 61 (2017) e02168–02116.
- [36] M. Yamaoka-Tojo, Vascular endothelial glycocalyx damage in COVID-19, *Int. J. Mol. Sci.* 21 (2020) 9712.
- [37] A.S. Johnston, R. Fatemi, W. Winlow, SARS-CoV-2 bound human serum albumin and systemic septic shock, *Front. Cardiovasc. Med.* 7 (2020).
- [38] M. Aziz, R. Fatima, W. Lee-Smith, R. Assaly, The association of low serum albumin level with severe COVID-19: a systematic review and meta-analysis, *Crit. Care* 24 (2020) 255.
- [39] S. Dirajlal-Fargo, M. Kulkarni, E. Bowman, L. Shan, A. Sattar, N. Funderburg, G. A. McComsey, Serum albumin is associated with higher inflammation and carotid atherosclerosis in treated human immunodeficiency virus infection, *Open Forum Infect. Dis.* 5 (2018).
- [40] A. Boulestin, N. Kamar, K. Sandres-Saune, L. Alric, J.P. Vinel, L. Rostaing, J. Izopet, Pegylation of IFN-alpha and antiviral activity, *J. Interferon Cytokine Res.* 26 (2006) 849–853.
- [41] L. Calandrelli, A. Calarco, P. Laurienzo, M. Malinconico, O. Petillo, G. Peluso, Compatibilized polymer blends based on PDLA and PCL for application in bioartificial liver, *Biomacromolecules* 9 (2008) 1527–1534.
- [42] J.-K. Sun, F. Sun, X. Wang, S.-T. Yuan, S.-Y. Zheng, X.-W. Mu, Risk factors and prognosis of hypoalbuminemia in surgical septic patients, *PeerJ* 3 (2015) e1267–e1267.
- [43] T. Loftsson, Cyclodextrins in parenteral formulations, *J. Pharm. Sci.* 110 (2021) 654–664.
- [44] Precision of internal standard and external standard methods in high performance liquid chromatography, *Special Issues* 33 (2015) 40–46.
- [45] G. Wang, K. Siggers, S. Zhang, H. Jiang, Z. Xu, R.F. Zernicke, J. Matyas, H. Uludağ, Preparation of BMP-2 containing bovine serum albumin (BSA) nanoparticles stabilized by polymer coating, *Pharm. Res.* 25 (2008) 2896–2909.
- [46] A. Lodagekar, R.M. Borkar, S. Thatikonda, R.B. Chavan, V.G.M. Naidu, N. R. Shastri, R. Srinivas, N. Chella, Formulation and evaluation of cyclodextrin complexes for improved anticancer activity of repurposed drug: niclosamide, *Carbohydr. Polym.* 212 (2019) 252–259.
- [47] S.K. Sahu, P. Zheng, N. Yao, Niclosamide blocks rice leaf blight by inhibiting biofilm formation of *Xanthomonas oryzae*, *Front. Plant Sci.* 9 (2018) 408.
- [48] S. Mandal, S.R. Prasad, D. Mandal, P. Das, Bovine serum albumin amplified reactive oxygen species generation from anthracycline-derived carbon dot and concomitant nanoassembly for combination antibiotic–photodynamic therapy application, *ACS Appl. Mater. Interfaces* 11 (2019) 33273–33284.
- [49] A.M. Alkilany, A.I. Bani Yaseen, M.H. Kailani, Synthesis of monodispersed gold nanoparticles with exceptional colloidal stability with grafted polyethylene glycol-polyvinyl alcohol, *J. Nanomater.* 2015 (2015), 712359.
- [50] A. Alfaro, A. León, E. Guajardo, P. Reuquen, F. Torres, M. Mery, R. Segura, P. A. Zapata, P.A. Orihuela, MgO nanoparticles coated with Polyethylene Glycol as carrier for 2-Methoxyestradiol anticancer drug, *bioRxiv* (2019), 588939.
- [51] N.N. Mahmoud, A.A. Alhusban, J.I. Ali, A.G. Al-Bakri, R. Hamed, E.A. Khalil, Preferential accumulation of phospholipid-PEG and cholesterol-PEG decorated gold nanorods into human skin layers and their photothermal-based antibacterial activity, *Sci. Rep.* 9 (2019) 5796.
- [52] X. Tang, Y. Liang, X. Liu, S. Zhou, L. Liu, F. Zhang, C. Xie, S. Cai, J. Wei, Y. Zhu, W. Hou, PLGA-PEG nanoparticles coated with anti-CD45RO and loaded with HDAC plus protease inhibitors activate latent HIV and inhibit viral spread, *Nanoscale Res. Lett.* 10 (2015) 413.
- [53] J. Cui, R. De Rose, K. Alt, S. Alcantara, B.M. Paterson, K. Liang, M. Hu, J. Richardson, Y. Yan, C.M. Jeffery, R.I. Price, K. Peter, C.E. Hagemeyer, P. S. Donnelly, S.J. Kent, F. Caruso, Engineering poly(ethylene glycol) particles for improved biodistribution, *ACS Nano* 9 (2015) 1571–1580.
- [54] R. Javed, M. Zia, S. Naz, S.O. Aisida, N.u. Ain, Q. Ao, Role of capping agents in the application of nanoparticles in biomedicine and environmental remediation: recent trends and future prospects, *J. Nanobiotechnol.* 18 (2020) 172.
- [55] M. Moïnour, N.K. Barker, L.E. Guzman, J.C. Jewett, P.R. Langlais, J.C. Schwartz, Discriminating changes in protein structure using tyrosine conjugation, *Protein Sci.* 29 (2020) 1784–1793.
- [56] S. Richard, V.L. Anton, B. Hans-Peter, A.E. Sergey, A.O. Alexander, Gold nanorod distribution in mouse tissues after intravenous injection monitored with optoacoustic tomography, *Proc. SPIE* (2011).
- [57] Y. Zhao, Y. Wang, F. Ran, Y. Cui, C. Liu, Q. Zhao, Y. Gao, D. Wang, S. Wang, A comparison between sphere and rod nanoparticles regarding their in vivo biological behavior and pharmacokinetics, *Sci. Rep.* 7 (2017) 4131.
- [58] K. Karami, N. Jamshidian, A. Hajiaghahi, Z. Amirghofran, BSA nanoparticles as controlled release carriers for isophthalaldoxime palladacycle complex; synthesis, characterization, in vitro evaluation, cytotoxicity and release kinetics analysis, *New J. Chem.* 44 (2020) 4394–4405.
- [59] Z. Yu, M. Yu, Z. Zhang, G. Hong, Q. Xiong, Bovine serum albumin nanoparticles as controlled release carrier for local drug delivery to the inner ear, *Nanoscale Res. Lett.* 9 (2014), 343–343.
- [60] A.G. Mares, G. Pacassoni, J.S. Marti, S. Pujals, L. Albertazzi, Formulation of tunable size PLGA-PEG nanoparticles for drug delivery using microfluidic technology, *PLoS One* 16 (2021), e0251821.
- [61] S.Y. Fam, C.F. Chee, C.Y. Yong, K.L. Ho, A.R. Mariatulqabtah, W.S. Tan, Stealth coating of nanoparticles in drug-delivery systems, *Nanomaterials* (Basel) 10 (2020).
- [62] C. Baraniuk, Covid-19: How effective are vaccines against the delta variant? *BMJ* 374 (2021) n1960.
- [63] Y. Liu, J. Rocklov, The reproductive number of the Delta variant of SARS-CoV-2 is far higher compared to the ancestral SARS-CoV-2 virus, *J. Travel Med.* (2021), taab124, <https://doi.org/10.1093/jtm/taab124>.
- [64] Predominance of Delta variant among the COVID-19 vaccinated and unvaccinated individuals, India, May 2021, *J. Infect.* (2021), <https://doi.org/10.1016/j.jinf.2021.08.006>.
- [65] C. Fu, C. Ding, X. Sun, A. Fu, Curcumin nanocapsules stabilized by bovine serum albumin-capped gold nanoclusters (BSA-AuNCs) for drug delivery and theranosis, *Mater. Sci. Eng. C* 87 (2018) 149–154.
- [66] W. Huang, C. Li, Z. Wang, H. Wang, N. Zhou, J. Jiang, L. Ni, X.A. Zhang, D.-W. Wang, Decreased serum albumin level indicates poor prognosis of COVID-19 patients: hepatic injury analysis from 2,623 hospitalized cases, *Sci. China Life Sci.* 63 (2020) 1678.
- [67] J. Huang, A. Cheng, R. Kumar, Y. Fang, G. Chen, Y. Zhu, S. Lin, Hypoalbuminemia predicts the outcome of COVID-19 independent of age and co-morbidity, *J. Med. Virol.* 92 (2020) 2152–2158.
- [68] S. Lim, J.H. Bae, H.-S. Kwon, M.A. Nauck, COVID-19 and diabetes mellitus: from pathophysiology to clinical management, *Nat. Rev. Endocrinol.* 17 (2021) 11–30.
- [69] M. Bansal, Cardiovascular disease and COVID-19, *Diabetes Metab. Syndr.* 14 (2020) 247–250.
- [70] T. Osada, M. Chen, X.Y. Yang, I. Spasojevic, J.B. Vandeusen, D. Hsu, B.M. Clary, T. M. Clay, W. Chen, M.A. Morse, H.K. Lyerly, Antihelminth compound niclosamide downregulates wnt signaling and elicits antitumor responses in tumors with activating APC mutations, *Cancer Res.* 71 (2011) 4172.
- [71] S. Anand, Y.S. Mayya, Size distribution of virus laden droplets from expiratory ejecta of infected subjects, *Sci. Rep.* 10 (2020) 21174.
- [72] C.-K. Lin, M.-Y. Bai, T.-M. Hu, Y.-C. Wang, T.-K. Chao, S.-J. Weng, R.-L. Huang, P.-H. Su, H.-C. Lai, Preclinical evaluation of a nanoformulated antihelminthic, niclosamide, in ovarian cancer, *Oncotarget* 7 (8) (2016).